Adsorption of Dansylated Amino Acids on Molecularly Imprinted Surfaces: A Surface Plasmon Resonance Study

*Xiao Li, Scott M. Husson**
Department of Chemical and Biomolecular Engineering, Clemson University, Clemson, SC 29634-0909
AUTHOR EMAIL ADDRESS: shusson@clemson.edu
* To whom correspondence should be addressed. Tel.: +1 (864) 656-4502. Fax: +1 (864) 656-0784. E-mail: shusson@clemson.edu.

Since mid-1980s, many biotechnology applications have explored the use of molecularly imprinted polymers (MIPs); largely, these have been applications for bioseparations and biosensing. For applications in biosensing, MIP-based biosensors possess considerable advantages compared to natural receptors, enzymes and antibody assays (e.g. ELISA). While the latter provide high specificities and affinities for binding target molecules, their chemical and thermal instabilities limit their application potential. Replacing natural recognition agents with MIPs offers technical, economic, and ethical advantages. They are easy to prepare at low cost, can withstand environments that would destroy natural antibodies, do not require animal-based production, and can be prepared for compounds (e.g., immunosuppressive agents) against which it is difficult to produce natural antibodies. With the enormous growth and growth potential for the biosensors market, a feasible technique is required to integrate MIPs with transducers and transform binding events between an MIP and its associated analyte into a processable signal.

SPR is an optical technique that measures changes in the refractive index of the medium near a metal surface. The sensing element comprises a recognition layer coated on a thin (~50 nm) film, typically of gold or silver, deposited on a glass substrate. Monochromatic, p-polarized light is reflected from the backside of the glass-gold interface. At a special angle of incidence known as the resonance angle, Θm, energy from the incident light is used to resonantly excite the surface plasmon at the gold-solution interface, which enhances the evanescent field. The value of Θm shifts with changes in the refractive index of the interfacial region adjacent to the gold surface (within approximately one-half the wavelength of the incident light). Therefore, SPR is a very sensitive technique for in situ measurement of interactions near the solution-solid interface. Rapid, label-free, high-sensitivity, real-time measurements are trademarks of SPR, making it a powerful tool for biomolecular interaction characterization. Recent applications of this technique include studies of biomolecule adsorption on self-assembled monolayers, biomolecule-polymer interactions and biokinetics.

Although a number of studies have explored the use of MIPs as recognition elements for applications in sensing, few molecular imprinting studies have applied the SPR technique. In this work, stable and inexpensive ultrathin MIP films (MIP-Fs) with recognition properties were prepared on SPR biosensor chips to create an optical MIP-based biosensor selective towards small biomolecules, and impact factors on binding interactions, including equilibration time, solution pH and polymer film thickness, were studied by SPR.

An important difference between this work and the few previously reported SPR-MIP biosensor studies is that atom transfer radical polymerization (ATRP) was used to grow polymer films *from the surface* by sequential addition of monomer from solution to surface-confined polymer chains. This approach contrasts those previous SPR-MIP biosensor

preparations that involve spin coating or other means of physical deposition methods. Our "grafting from" approach using ATRP provides advantages: it produces high polymer segment densities that shield the underlying substrate, and it forms highly uniform polymer surfaces with controllable layer thicknesses at the nanoscale (< 15 nm). Since polymer surface chemistry must be reproducible and free of defects for meaningful SPR analysis, these advantages make graft ATRP a desirable method for SPR-biosensor preparations.

Experiment methods

Preparation of initiator-functionalized surfaces and surface-confined polymer films (Scheme 1). The gold substrates were cleaned with fresh Piranha solution and modified by a thiol self-assembled monolayer (SAM) of MUD. The SAM provides hydroxyl functional groups that were reacted with (4-chloromethyl)benzoyl chloride to create an initiator-functionalized layer. Room temperature molecular imprinting polymerization was carried out from the surface-confined initiator sites using 2-Vpy as functional monomer and EGDMA as cross-linking monomer. The solvent was acetonitrile. The MIP-F surfaces were prepared by adding the template, DDC or DDL, into the polymerization solution. Non-imprinted polymers (NIP-Fs) were prepared as controls; polymerization of NIP-Fs was done under exactly the same conditions, but with no template in solution.

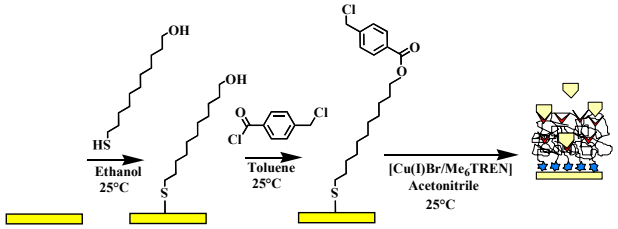

Scheme 1. Strategy for preparing 2-D MIP films on gold substrates.

Results and Discussion

The surface was characterized by ellipsometry and ER-FTIR measurements after each reaction step. Figure 1 presents typical reflectance FTIR spectra for SAM, initiator-functionalized SAM, and polymer films. Previous XPS results and AFM also proved the similarities of MIP-F and NIP-F in both surface composition and topography. It is important for our study on dansylated amino acid adsorption. Since the template molecules will see comparably the same surfaces in rebinding experiments, any enhancement seen in template binding capacity or affinity for the MIP-F cannot be attributed to differences in the surface composition or roughness, but, rather, differences must be attributed to an imprinting effect.

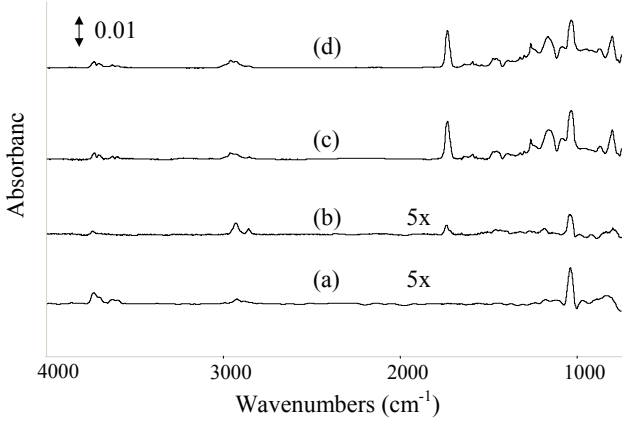

Figure 1. External Reflectance FTIR spectra on gold substrate: (a) 11-Mercapto-undecanol SAM; (b) grafted (4-chloromethyl)benzoyl chloride initiator on SAM; (c) grafted MIP-F poly(2-vinylpyridine-co-EGDMA)(0.1:12:40) layer (70 Å); (d) grafted NIP-F poly(2-vinylpyridine-co-EGDMA)(12:40) layer (85 Å). The template molecule was N,N'-didansyl-L-cystine (DDC) The spectra of SAM and initiator were amplified 5X.

Figure 2a shows an example SPR sensorgram for DDL adsorption on MIP-F surface with a template (DDL):2-Vpy:EGDMA molar ratio of 0.1:12:40. Upon injection of analyte-containing solution over the surface, there was a rapid signal response due to differences in the refractive indices of the buffer and analyte solution (1000 RU is a change in resonance angle of 0.1° and corresponds to a change in the index of refraction in solution of 0.0011 [BIAcore AB, 1997]), followed by a slower increase as the DDL adsorbed to the surface, eventually approaching the equilibrium binding amount. By reintroduction of buffer into the flow cell, there was an immediate drop in the SPR signal due to refractive index switching, as well as the desorption of template molecules from the surface. Figure 2b shows a complete cycle of sample injection and surface regeneration. The response returned to its original baseline value after high-speed buffer wash and regeneration; therefore, it is possible to remove the template molecule from the polymer with 100% efficiency. Similar findings for DDC indicate that no measurable amount of DDC, which has a disulfide group, was able to interact with the MIP-F-coated gold surface. This finding suggests that the film provided uniform, dense coverage of the substrate over the region that was sampled by SPR.

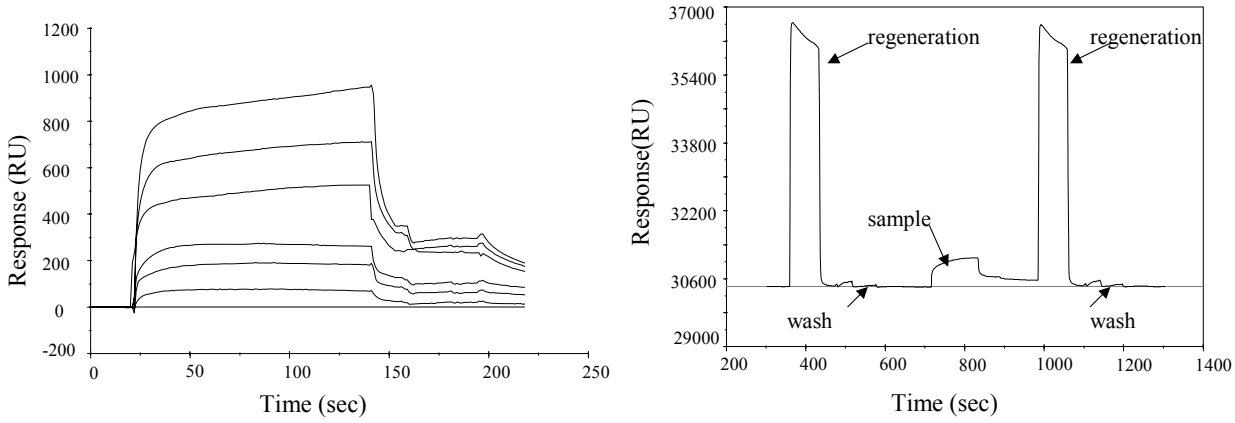

a b

Figure 1. SPR sensorgrams of didansyl-L-lysine (DDL) adsorption on MIP-F (70 Å) surface with a template (DDL):2-Vpy:EGDMA molar ratio of 0.1:12:40 at T = 25 °C. a. Sensorgrams run at different concentrations of DDL (in mg/ml) in HEPES buffer of pH 7.8: 0.01, 0.025, 0.05, 0.1, 0.2, and 0.3. Flow rate was 20 µl/min. Buffer shift has been subtracted. b. Entire sensorgram cycle showing sample injection, regeneration and high-speed buffer wash. The horizontal line is the base line.

The entire adsorption process of template molecules onto a MIP-F (NIP-F) surface involves template external mass transfer to the solution-film interface, interfilm mass transfer to binding sites, and site-binding ("reaction") on the surface. In Figure 2, the initial binding responses obtained in SPR measurements at different flow rates were used to examine the diffusion of template molecules to the copolymer surface. We found that the binding rate was

independent of flow rate, suggesting that the DDC-MIP-F (NIP-F) interaction was not limited by external mass transfer to the film surface.

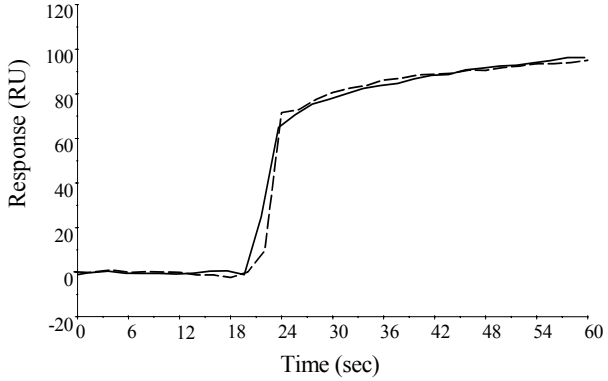

Figure 2. SPR sensorgram of initial binding response for 0.3 mg/mL of N,N'-didansyl-L-cystine (DDC) adsorbing to the MIP-F surface (70 Å) prepared with template (DDC):2-Vpy:EGDMA molar ratio of 0.1:12:40 at different flow rates: 5 μl/min (dash line) and 20 μl/min (solid line). The solvent was 10 mM HEPES buffer at pH = 7.0. Buffer shift has been subtracted.

To test whether adsorption was controlled by the reaction kinetics or by interfilm mass transport, we estimated the time constants for interfilm diffusion and binding using Equations 1 and 2,

$$\tau_D = \frac{h^2}{6D} \qquad [1]$$

$$\tau_B = \frac{1}{k_a \cdot [C]} \qquad [2]$$

where h is film thickness, D is the interfilm diffusion coefficient, k_a is the association (reaction) rate constant and [C] is the concentration of dansylated amino acid. If reactive binding is the limiting step, τ_D should be much smaller than τ_B. Due to the unavailability of diffusion coefficient data for similar diffusants in highly crosslinked polymers, we estimated a value for the diffusion coefficient that would give a time constant for interfilm diffusion that was two orders of magnitude lower than that for reactive binding. From Equation 2, τ_B was calculated using k_a values obtained by fitting SPR data to Langmuir models. For τ_D to be two orders of magnitude lower than τ_B, D was estimated to be ~5 × 10^{-12} cm^2/s in our system. Such a low value of D suggests that reactive binding is the limiting step in our adsorption studies. This analysis demonstrates the importance of creating ultrathin layers, with thicknesses < 10 nm, to avoid interfilm diffusional mass transfer limitations in real-time biosensing applications. For example, an increase in film thickness to just 100 nm would increase the calculated D by 100-fold to 10^{-10} cm^2/s, which is equal to the magnitude for diffusion of small molecules in solids. So, for relatively larger molecules diffusing in our crosslinked film, we would likely be diffusion limited at 100 nm.

This result supports that a simple bimolecular interaction model, is appropriate to describe the DDC-MIP-F (NIP-F) interaction. The binding kinetics data were first fitted to a simple single-site Langmuir adsorption model (Figure 3, dotted curves). Equations 3 - 6 show the simple bimolecular interaction and the corresponding rate equation.

$$A + S \underset{k_d}{\overset{k_a}{\longleftrightarrow}} AS \qquad [3]$$

$$\frac{d[AS]}{dt} = k_a[A][S] - k_d[AS] \quad [4]$$

$$AS \xrightarrow{k_d} A + S \quad [5]$$

$$-\frac{d[AS]}{dt} = k_d[AS] \quad [6]$$

In integrated form described by SPR parameters, the rate equations are

$$\text{Association: } Q = \frac{[A]k_a Q_{max}[1 - e^{-([A]k_a + k_d)t}]}{[A]k_a + k_d} \quad [7]$$

$$\text{Dissociation: } Q = Q_{max} e^{-k_d(t - t_0)} \quad [8]$$

where Q is the surface uptake measured by SPR and Q_{max} is the response at start time of dissociation t_0. **Table 1** summarizes the results from data regression using this single-site binding model. By fitting the experiment data with the single-site Langmuir binding model, a low correlation coefficient ($R^2 < 0.9$) was observed for adsorption on MIP-F with high functional monomer content, while fits were somewhat better to data for NIP-F surfaces and MIP-F with low functional monomer content. Past findings have demonstrated that imprinted materials display more heterogeneous binding than NIPs. The results for the MIP-F/NIP-F set with 12:40 functional monomer:crosslinker ratio suggest the same. While the goodness of fit were the same for the MIP-F/NIP-F set with 3:40 monomer ratio, the fit was improved substantially by allowing more than one type of binding site (vide infra).

Table 1. Comparison of the adsorption rate constants and equilibrium adsorption capacities (Q_{max}) for single-site and dual-site Langmuir adsorption models. The experiments examined the adsorption of 0.1 mg/mL to 0.6 mg/mL DDC on MIP-F and NIP-F. Template (DDC):2-Vpy:EGDMA molar ratio are 0.1:3:40 (with thicknesses for MIP-F (0.1:3:40) and NIP-F (3:40) of 59 ± 3 Å and 57 ± 2 Å, respectively) and 0.1:12:40 (with thicknesses for MIP-F (0.1:12:40) and NIP-F (12:40) of 70 ± 2 Å and 85 ± 3 Å, respectively). The solvent was 10 mM HEPES buffer at pH = 7.0. Units: k_a [M^{-1} s^{-1}], k_d [s^{-1}], Q_{max} [pmoles/cm^2·Å].

Surfaces	single-site model				dual-site model						
	k_a	k_d	Q_{max}	R^2	k_{a1}	k_{d1}	Q_{max1}	k_{a2}	k_{d2}	Q_{max2}	R^2
MIP(0.1:3:40)	301.8	0.06	0.93	0.94	401.2	0.6	0.79	17.4	1.0×10^{-2}	0.53	1.0
NIP(3:40)	63.2	0.09	1.15	0.93	87.0	0.4	0.98	16.3	4.7×10^{-3}	0.53	0.99
MIP(0.1:12:40)	204.8	0.05	0.83	0.87	455.2	0.3	0.45	26.7	5.3×10^{-3}	0.63	0.99
NIP(12:40)	211.7	0.03	0.61	0.92	311.4	0.6	0.22	11.7	3.3×10^{-3}	0.31	0.97

To improve the binding kinetics model, and to test whether binding site heterogeneity might account for lack of fit with the Langmuir model, a dual-site Langmuir adsorption model was used to describe the experiment data (Figure 3, solid curves). In this model, two binding sites offering different binding interactions were postulated to exist in the copolymer surface films. Equations 9 - 12 give the reactions and the rate expressions for the dual-site Langmuir model.

$$A + S1 \underset{k_{d1}}{\overset{k_{a1}}{\longleftrightarrow}} AS1 \qquad A + S2 \underset{k_{d2}}{\overset{k_{a2}}{\longleftrightarrow}} AS2 \quad [9]$$

$$\frac{d[AS1]}{dt} = k_{a1}[A][S1] - k_{d1}[AS1] \qquad \frac{d[AS2]}{dt} = k_{a2}[A][S2] - k_{d2}[AS2] \quad [10]$$

$$AS1 \xrightarrow{k_{d1}} A + S1 \qquad AS2 \xrightarrow{k_{d2}} A + S2 \qquad [11]$$

$$-\frac{d[AS1]}{dt} = k_{d1}[AS1] \qquad -\frac{d[AS2]}{dt} = k_{d2}[AS2] \qquad [12]$$

Experimental adsorption kinetics data were modeled as the sum of two integrated rate equations, as shown in Equations 13 and 14.

$$\text{Association: } Q = \frac{[A]k_{a1}Q_{max1}[1-e^{-([A]k_{a1}+k_{d1})t}]}{[A]k_{a1}+k_{d1}} + \frac{[A]k_{a2}Q_{max2}[1-e^{-([A]k_{a2}+k_{d2})t}]}{[A]k_{a2}+k_{d2}} \qquad [13]$$

$$\text{Dissociation: } Q = Q_{max1}e^{-k_{d1}(t-t_0)} + Q_{max2}e^{-k_{d2}(t-t_0)} \qquad [14]$$

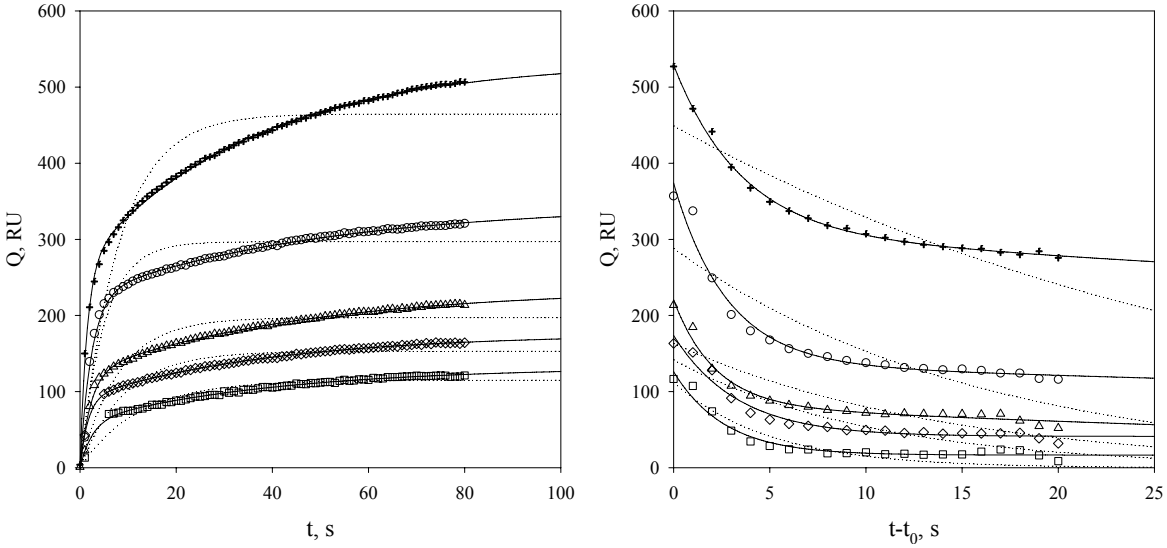

Figure 3. Binding kinetics of N,N'-didansyl-L-cystine (DDC) on MIP-F surfaces (70 Å) using SPR. Left: association over the first 80 s; Right: dissociation over the first 20 s (t_0 = 140 s in the experiments described). Data (symbols) were fit to a single-site Langmuir adsorption model (dotted curves) and a dual-site Langmuir adsorption model (solid curves). The concentrations of free template molecules DDC (in mg/ml) were 0.1 (□), 0.2 (◊), 0.3 (Δ), 0.5 (o), and 0.6 (+). Flow rate was 20 μl/min. Buffer shift and bulk response were subtracted from original sensorgram. The solvent was 10 mM HEPES buffer at pH = 7.0.

Figure 3 demonstrates clearly that the dual-site Langmuir binding model more accurately describes the template molecule rebinding on molecularly imprinted polymer surfaces, likely due to the heterogeneity of binding sites formed in the polymer film. Higher-order binding site models continuous distribution models, such as the Freundlich or Langmuir-Freundlich models, are likely to describe the data slightly more accurately than the dual-site model. However, increasing the number of independent binding site types comes with the price of increasing the number of adjustable fitting parameters and, for the latter models, additional model complexity.

Equilibrium Isotherm Models. In this work, four isotherm models were examined to describe the equilibrium data: Langmuir, dual-site Langmuir, Freundlich, and Langmuir-Freundlich (LF):

$$\text{Langmuir: } Q = \frac{Q_{max} \cdot [A]}{K_d + [A]} \qquad [15]$$

dual-site Langmuir: $$Q = \frac{Q_{max1} \cdot [A]}{K_{d1} + [A]} + \frac{Q_{max2} \cdot [A]}{K_{d2} + [A]} \quad [16]$$

Freundlich: $$Q = Q_{max}[A]^m \quad [17]$$

Langmuir-Freundlich: $$Q = \frac{Q_{max} \cdot [A]^m}{K_d + [A]^m} \quad [18]$$

Additional parameters not defined previously are the equilibrium dissociation constants (K_d) and heterogeneity index (m).

Figure 4 presents the quantitative results of DDL adsorption on MIP-F and NIP-F surfaces. Curves represent fits of the data to Langmuir, dual-site Langmuir, Freundlich, and Langmuir-Freundlich (LF) isotherm models. (Also see **Tables 2** and **3** for parameter details.) Surprisingly, although the Scatchard plots showed surface heterogeneity, the adsorption isotherms could be well expressed by the simplest Langmuir model.

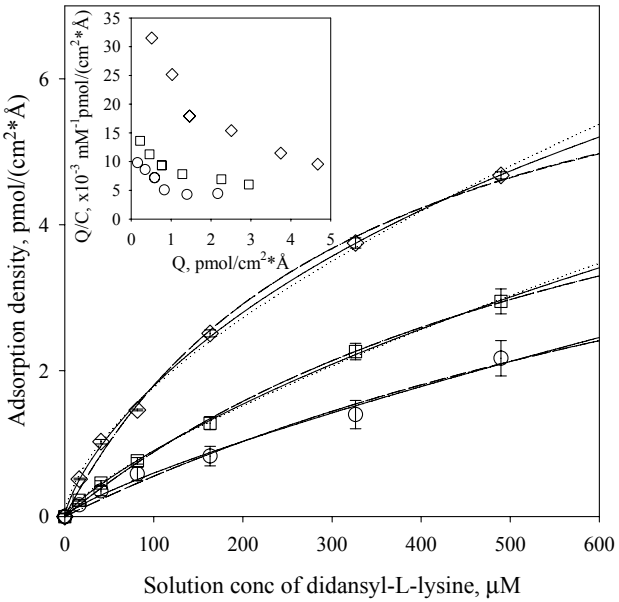

Figure 4. Adsorption isotherms for DDL on NIP-F (○) and MIP-F (0.1:12:40) prepared with DDL (◊) or DDC ( ) as the template. Curves represent fits to the Langmuir (dash), dual-site Langmuir (dash-dot), Freundlich (dotted), and Langmuir-Freundlich (solid) isotherm models. Insert: Scatchard plot. The thicknesses for MIP-F prepared against DDC, MIP-F prepared against DDL and NIP-F were 70 ± 2 Å, 32 ± 2 Å and 85 ± 3 Å, respectively. The solvent is 10 mM HEPES buffer at pH = 7.8. Surface adsorbed amount (in RU) has been converted to pmol/(cm^2·Å) by dividing the thickness (Å) of polymer films.

For this set of materials, at all solution concentrations, MIP-F surfaces demonstrate higher binding capacity than NIP-Fs. A selectivity coefficient was defined as

$$\alpha_{DDL,DDC} = \frac{K^*_{DDL,MIP} / K^*_{DDL,NIP}}{K^*_{DDC,MIP} / K^*_{DDC,NIP}}$$

where K* represent the initial slope values for the adsorption isotherms. Table 2 gives the fitted K* and α values for MIP-F surfaces prepared against DDC and DDL at the neutral pH (7.0) adsorption condition. The selectivity coefficient is 1.40 for MIP-F surface with DDC as the

template molecule (MIP-DDC) and 1.11 for DDL as the template (MIP-DDL). The higher selectivity indicates that MIP-DDC has stronger specific binding of its own template molecule than does MIP-DDL. The results also display some cross-reactivity between these two molecules. That is, adsorption of DDL onto MIP-DDC was higher than adsorption onto the NIP-F. Similarly, adsorption of DDC onto MIP-DDL was higher than adsorption onto the NIP-F.

Table 2. Fitted parameters for the Langmuir model determined by regression of MIP-F and NIP-F adsorption isotherm data. The thicknesses for MIP-F prepared against DDC, MIP-F prepared against DDL and NIP-F were 70 ± 2 Å, 32 ± 2 Å and 85 ± 3 Å, respectively. The pH was 7.0.

Template: N,N'-didansyl-L-cystine (DDC)				
	Q_{max} (pmoles/cm^2·Å)	K (μM^{-1}) × 10^4	K^* (pmoles/cm^2·Å·μM)	α
DDC on MIP-DDC	2.29	6.38	1.46×10^{-3}	1.40
DDC on NIP	0.86	8.96	7.68×10^{-4}	
DDL on MIP-DDC	3.30	29.66	9.77×10^{-3}	
DDL on NIP	2.82	25.45	7.17×10^{-3}	
Template: Didansyl-L-lysine (DDL)				
	Q_{max} (pmoles/cm^2·Å)	K (μM^{-1}) × 10^4	K^* (pmoles/cm^2·Å·μM)	α
DDL on MIP-DDL	4.53	60.98	2.76×10^{-2}	1.11
DDL on NIP	2.82	25.45	7.17×10^{-3}	
DDC on MIP-DDL	1.87	14.33	2.68×10^{-3}	
DDC on NIP	0.86	8.96	7.68×10^{-4}	

Usually, optimum template rebinding occurs under the same conditions used during the polymerization to produce the MIP. Changing the environmental conditions impacts cavity shape and the distance between functional groups in the polymer matrix, which may result in loss of MIP's specificity for rebinding their templates. Therefore, we compared the adsorption isotherms of these two MIP-F surfaces to data from our previous adsorption studies, which used fluorometry as the characterization method and acetonitrile as the rebinding solvent. We found that selectivities differed by < 8 % between the two solvent systems; but adsorption capacities of DDC were 40 % lower in aqueous solution, whereas adsorption capacities for DDL were 10 % higher in aqueous solution. The ability to maintain (and even increase) selective binding capacities in aqueous solution will benefit the application of such an MIP-F in biosensing, where aqueous environments are used widely for in vivo or in vitro biomolecule detection systems.

Table 3 compares regression statistics for the Langmuir, dual-site Langmuir, Freundlich and Langmuir-Freundlich (LF) binding models. Overall, R^2 values were high ($R^2 > 0.95$) for all four models under all conditions studied. Heterogeneous binding models did show slight improvement for adsorption of DDC, while R^2 remains high (>0.99) for all DDL adsorptions. In contrast to the kinetic data regression that showed clear differences for Langmuir and dual-site Langmuir models, description of the equilibrium data was less sensitive to model choice. One hypothesis relates to the heterogeneity of polymer surfaces: The inability of the single-site Langmuir model to describe the kinetics data may be attributed to the fact that sites with low binding energies adsorb/release the template at different rates than sites with higher binding energies. Therefore, site heterogeneity may impact kinetics fittings with higher sensitivity than equilibrium isotherm fittings.

Table 3. Fitted binding parameters and corresponding correlation coefficient using Langmuir dual-site Langmuir, Freundlich, and Langmuir-Freundlich (LF) isotherm models. Units: K^* [pmoles/cm^2·Å·μM] $\times 10^3$.

DDC on MIP (DDC)

	Langmuir		Dual-site Langmuir		Freundlich		LF		
pH	K*	R^2	K*	R^2	m	R^2	K*	m	R^2
6.4	3.95	1.0	3.95	1.0	0.79	1.0	10.30	0.79	1.0
7.0	1.46	0.95	1.46	0.95	0.74	0.96	5.52	0.74	0.96
7.8	0.74	0.96	0.74	0.96	0.63	0.97	4.93	0.63	0.97

DDC on NIP

	Langmuir		Dual-site Langmuir		Freundlich		LF		
pH	K*	R^2	K*	R^2	m	R^2	K*	m	R^2
6.4	1.25	0.99	1.25	0.99	0.87	0.99	2.29	0.87	0.99
7.0	0.77	0.98	0.77	0.98	0.71	0.99	3.16	0.71	0.99
7.8	0.60	0.96	0.60	0.96	0.67	0.98	3.42	0.67	0.98

DDL on MIP (DDL)

	Langmuir		Dual-site Langmuir		Freundlich		LF		
pH	K*	R^2	K*	R^2	m	R^2	K*	m	R^2
6.4	38.41	1.0	38.41	1.0	0.53	1.0	70.46	0.80	1.0
7.0	27.60	0.99	27.60	0.99	0.71	1.0	64.92	0.71	1.0
7.8	23.42	1.0	23.43	1.0	0.62	1.0	64.33	0.75	1.0

DDL on NIP

	Langmuir		Dual-site Langmuir		Freundlich		LF		
pH	K*	R^2	K*	R^2	m	R^2	K*	m	R^2
6.4	12.11	1.0	12.11	0.99	0.64	1.0	16.67	0.90	1.0
7.0	7.165	1.0	7.165	0.98	0.85	1.0	8.971	0.93	1.0
7.8	5.985	0.98	5.989	0.96	0.79	0.99	15.69	0.79	0.99

The binding of template biomolecules on MIP-F/NIP-F surfaces is impacted significantly by polymer properties (composition, layer thickness), as well as the measurement environment (pH, temperature, ionic strength) and interaction time. In this study, our objective was to determine the effects of layer thickness and solution pH on adsorption properties.

Figure 5 shows the adsorption density of DDC on MIP-F and NIP-F surfaces with two different polymer thicknesses. The similar values of adsorption density indicate a linear dependence of template adsorption amount on polymer thickness. This finding suggests a relatively homogenous distribution of binding sites exists along the polymer growth direction within the polymer films. Also, this result shows that, by dividing the areal uptake capacity obtained in SPR measurements by polymer layer thickness, it is possible to compare binding capacities of polymer surfaces with various layer thicknesses. We believe that the adsorption density is more representative than areal uptakes, since interactions between template molecules and imprint cavities happen at the surface and also within the polymer layer.

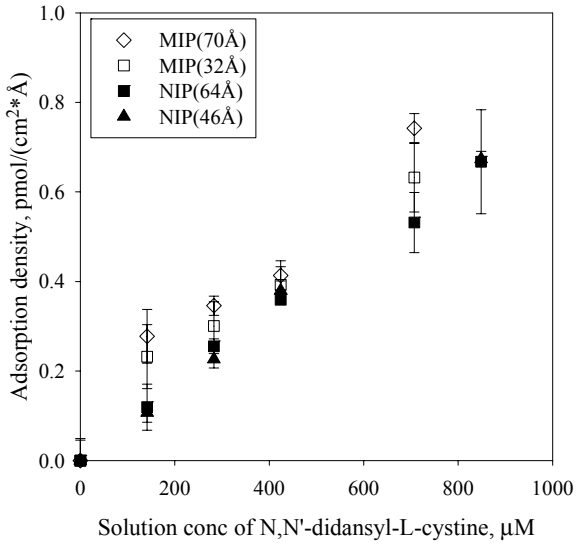

Figure 5. Polymer thickness dependence of DDC adsorption on MIP-F (0.1:12:40) and NIP-F (12:40) surfaces. The solvent was 10 mM HEPES buffer at pH = 7.0.

Figure 6 presents adsorption isotherms for DDC and DDL on MIP-F and NIP-F surfaces at three pH values. We consistently saw higher surface adsorption densities for DDL compared to DDC. This difference is likely due to differences in the activities of these two compounds in water caused by differences in their molecular structures. Compared to DDL, which only has one acid group, DDC, which has two acid groups, is likely more hydrophilic.

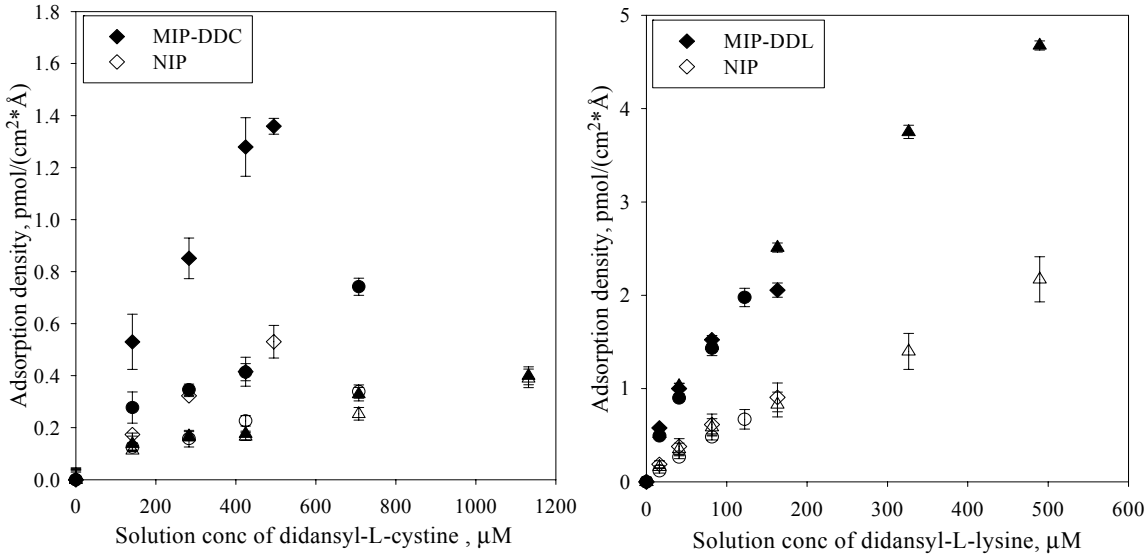

(a) (b)

Figure 6. Adsorption studies of didansyl-L-cystine (DDC) (a) and didansyl-L-lysine (DDL) (b) on MIP-DDC, MIP-DDL and NIP-F surfaces at pH 6.4 (diamond), 7.0 (circle), and 7.8 (triangle). The solvent was 10 mM HEPES buffer adjusted to pH using NaOH (50% w/w in H_2O).

Figure 7 shows the dependence of binding selectivity coefficient on solution pH for MIP-Fs formed with the two template molecules. Interestingly, the selectivity of MIP-DDC decreased with increasing pH value, whereas MIP-DDL increased with increasing pH. Moreover, adsorption of the MIP-DDC is more sensitive to pH than MIP-DDL. In order to better

understand the microenvironment in our binding measurements, pK_a values of these two template molecules were measured by potentiometric titrations. While we expected to find two independent pK_a values for the acid groups of DDC, instead we found single inflection points for both DDC and DDL that gave pK_a values of 6.2 for both compounds. Hence, under all three pH conditions, most of the biomolecules exist in their deprotonated form. The approximate fraction of molecules in the deprotonated form was calculated as 61.3% for pH 6.4, 86.4% for pH 7.0, and 97.6% for pH 7.8, respectively. We measured the pK_a of poly(2-vinylpyridine) as 5.0 ± 0.1, which means that essentially all of the pyridine groups exist in non-protonated, non-ionic form at these solution pH conditions. Therefore, under the conditions used in this study, the adsorption of template on MIP-F (NIP-F) surface could be the result of hydrophobic (dispersive) interactions and hydrogen bonding (at the low pH value).

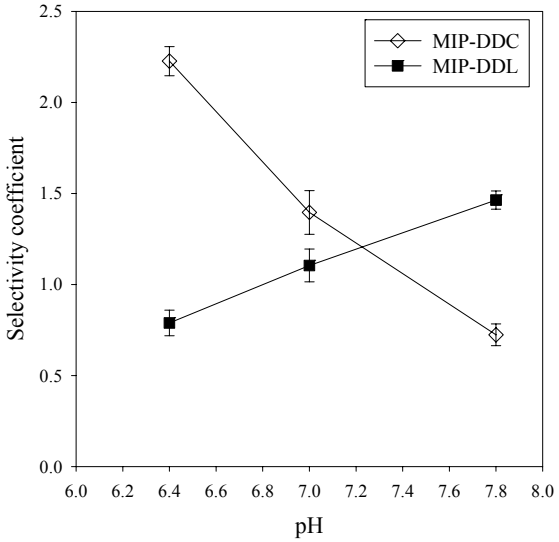

Figure 7. Effect of the pH on the selectivity of DDC and DDL-MIP-F surfaces, analysis using Langmuir isotherm.

A few reports have described pH effects on rebinding template with MIPs, including those that describe pH-dependent affinity of imprinted metal complex binding sites or intelligent imprinted hydrogels. In this work, we demonstrated that SPR can be used to measure the pH-dependence of adsorption of charged analytes on ultrathin MIP films. Given the results of our study, and studies that have shown the influence of pH on the swelling behavior of MIP materials and its influence on recognition properties, we believe that pH changes represent a promising way to tune the selectivity of aqueous MIP systems involving ionizable analytes and/or monomer units.

Conclusions

ATRP graft polymerization was used to prepare uniform polymer surfaces for biomolecule adsorption studies by SPR. Imprinted and non-imprinted polymer films were grown from SPR sensing elements (gold). The controllable nature of ATRP allowed the growth of uniform MIP films with adjustable thicknesses, preventing diffusional mass transfer limitations from affecting the kinetic analysis. ATRP is therefore well-suited to prepare MIP films as recognition elements for applications in biosensors.

SPR measured higher adsorption capacities for imprinted films relative to non-imprinted films when high percentage of functional monomer was used in polymer synthesis. Cross-reactivity was seen between similar template compounds, but MIP-Fs showed selective binding, and the selectivity changed with solution pH values. Kinetic models were compared that incorporated first-order interactions with single-site and dual-site binding. Impact factors that were studied included solution pH, polymer thickness and interaction time. Adsorption capacity was found to scale with polymer layer thickness, i.e., adsorption density was found to be independent of layer thickness. This result suggests that films of different thicknesses can be compared by appropriate normalization.

While this study used fluorescently-labeled analytes, the methodology used to prepare the films applies also to non-fluorescent templates of interest in many environmental or biological samples. This methodology can also be extended to other substrate geometries and chemistries.